Proceedings of ICFDP7
Seventh International Conference of Fluid Dynamics and Propulsion
December 18-20, 2001 Cairo, EGYPT

ICFDP7-2001043

ON THE SHOCK INTERACTION WITH A VORTEX RING

Mohammed Y. Hussaini*
Florida State University
Tallahassee, Florida 32306-4120
Email: myh@csit.fsu.edu

Zhong Ding
Florida State University
Tallahassee, Florida 32306-4120
Email: ding@csit.fsu.edu

Gordon Erlebacher
Florida State University
Tallahassee, FL 32306-4120
Email: erlebach@math.fsu.edu

ABSTRACT
The interaction of a vortex ring with a plane shock is investigated numerically in the framework of the axisymmetric Euler equations. The numerical experiments consider a range of circulations and shock Mach numbers.

Keywords: compressible, acoustics, fluids, shocks, vortex ring, numerical methods.

INTRODUCTION
A vortex ring embodies various essential characteristics of vortical motion. As Saffman [1] put it, "One particular motion exemplifies the whole range of problems of vortex motion and is also a commonly known phenomenon, namely, the vortex ring or smoke ring." Vortex rings are commonly observed in axisymmetric jets and wakes. As they are easy to generate and analyze, they have been the subject of extensive studies, particularly with reference to the issues of sound generation [2-4], transport and mixing [5-7], and vortex interactions [8-10]. An excellent review on the subject is provided by Shariff and Leonard [8]. Recently, there have been several studies on the phenomena of a shock interacting with a vortex ring [2-4, 9-13]. Such phenomena are observed in high-speed aerodynamic flows [14,10] and automobile exhaust flow-fields [15-17]. These studies are mainly motivated by the noise generation aspect of the shock-vortex ring interaction.

The experiments on 'clean' shock/vortex ring interactions [10, 12, 13], revealed the resultant shock diffraction and refraction patterns, density variations across the vortex core, and the velocity of the shock. The last study also observed the generation of complex acoustic wave patterns centered on the transmitted vortex core. As this acoustic wave propagates, it intersects with itself on the axis of symmetry of the ring. However, all these investigations were qualitative in nature based on shadowgraphs and Schlieren pictures, but did not provide quantitative information.

The computational study of Takayama *et al*. [17] that simulated the experiment of Minota [10] showed significant distortion of the shock, including shock bifurcation and the generation of several triple points. The triple points converged at the symmetry axis, resulting in a very high compression peak which was over ten times that of the upstream mean pressure. However, this large pressure peak was not observed in any experimental study. The experimental and numerical studies of Minota *et al*. [4] of a similar flow configuration revealed shock bifurcation. However, the amplitude of the high pressure due to the converging triple points was only 75% of the upstream mean pressure. This result differs significantly from that of Takayama *et al*. [11].

A numerical study of the interaction of a plane shock with a vortex ring showed that the sound intensity was highly directional, and that the sound pressure level increased significantly with the shock strength [3]. Most importantly, the simulations showed that the relationship between the sound pressure level and the shock strength was consistent with the experimental observation of shock noise in supersonic jets [18], indicating thereby that the shock/vortex ring interaction correctly modeled a dominant mechanism of shock noise generation. The study was confined to the case of a single aspect ratio $R = 250$ (R is the ratio of the vortex-ring diameter to the vortex-core radius), an upstream Mach number of 1.5, and circulations $\Gamma = 0.75$ and 1.5 (within the *nonlinear* regime). This study omitted any discussion of features related

* Address all correspondence to this author.

to the axisymmetric nature of the configuration, in particular, the self-interaction of the toroidal sound wave. This was perhaps due to the fact that the aspect ratio of the vortex ring was relatively large so that the flow was essentially two-dimensional and that furthermore, the resolution was inadequate near the axis of symmetry to resolve the sound wave self-interaction phenomenon.

Shock/vortex ring interaction phenomena are also present in the exhaust system of an internal combustion engine [17]. Endo *et al* [16] used a pulsatile jet discharged from a pipe to model the periodic opening and closing of the exhaust valve of reciprocating internal combustion engines. They showed that the periodic vortex rings and shocks thus generated were responsible for spike-like noise. Futagami *et al*. [15] studied noise due to the pulsating flow through a pipe. They observed that the motion of the compression wave in the exhaust system has significant influence on the exhaust noise.

Recently, Ding, Hussaini and Erlebacher [19] studied the interaction of a vortex ring using highly accurate numerical simulations. Their emphasis was on the effects of axisymmetry on the generation of acoustic waves downstream of the shock. The simulation results show that the shock compresses the vortex core in the streamwise direction by a factor proportional to the ratio of the downstream and upstream mean velocities. In addition to vorticity and entropy disturbances, a toroidal acoustic wave is also generated. They found that as the downstream acoustic wave propagates outward from its source, its self-intersection on the symmetry axis leads to a strong intensification of the perturbation pressure levels. The amplitudes of these pressure peaks are found to increase as the aspect ratio of the vortex ring decreases. In this paper, we examine the effect of shock strength and upstream circulation strength on the structure of the shock, the downstream circulation, and the downstream pressure field.

NOMENCLATURE

M_1	:	Upstream Mach number
$R = 2r_c$	:	Ring aspect ratio
s	:	Entropy
(ρ_1, U_1, p_1)	:	Upstream density, streamwise velocity, pressure
(u'_1, v'_1, p'_1)	:	Upstream perturbation variables
(x, r)	:	Cylindrical coordinate system
(x_c, r_c)	:	Center of vortex core
δ	:	Shock displacement
Γ	:	Upstream circulation
Γ_2	:	Downstream circulation

PROBLEM FORMULATION

We study the interaction of a planar supersonic shock of infinite extent with a stationary axisymmetric vortex ring. The geometry is illustrated in Figure 1. The vortex ring has a diameter D and a core radius r_0. Its axis of symmetry is normal to the mean shock. In a cylindrical coordinate system (x, r), the symmetry axis is located at $r = 0$. Outside the core of the vortex, the flow is assumed to be irrotational. The circulation around the core is denoted by Γ_1. Rather than work in the frame of reference of the stationary vortex, we adopt a coordinate system attached to the mean shock location. Thus, $x = 0$ describes the shock profile prior to interaction with the vortex, which now convects at constant mean velocity U_1 towards the shock. Note that in a reference frame where positive x is upstream of the shock, the mean velocity U_1 is negative.

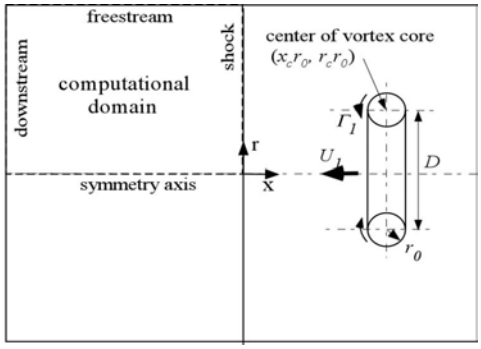

Figure 1. Schematic of the mathematical model.

The flow is assumed to be an inviscid ideal gas flow governed by the axisymmetric unsteady compressible Euler equations. All the variables have been non-dimensionalized in what follows. Pressure and density are normalized with respect to the mean upstream pressure P_1 and density ρ_1. Velocities are made non-dimensional with respect to $U = \sqrt{P_1/\rho_1}$, lengths with respect to the vortex core radius r_0, time with respect to r_0/U, and circulation Γ with respect to $r_0 U$. The time variable, denoted by t^*, is zero when the center of the vortex intersects the mean position of the shock. The leading and trailing edges of the vortical upstream region intersect the shock at $t^* = -1$ and $+1$ respectively. The entropy of the fluid, $s = \log\left[p/\rho^{\gamma}\right]$, is computed from the equation of state with a ratio of specific heats, $\gamma = 1.4$. Upstream of the shock, $u_1 = (U_1 + u'_1, v'_1)$, $p_1 = P_1(1 + p'_1)$, and $U_1 = M_1\sqrt{\gamma}$. The disturbance quantities u'_1, v'_1, p'_1 are defined by Lamb's formula [20]. The density is computed from the isentropic relation $\rho = \text{const.}\, p^{1/\gamma}$. The intersection of the vortex ring with an azimuthal plane is a pair of counter-rotating vortices (Figure 1). In non-dimensional units, the vortex has a circular core of unit radius, beyond which the flow is irrotational. The center of the core is located at (x_c, r_c), and has a circulation Γ. The vortex ring has an aspect ratio $R = 2r_c$. Precise expressions for the velocity and pressure disturbance fields associated with the vortex ring can be found in Ding *et al*. (19). All the results in this paper correspond to a vortex aspect ratio $R = 100$.

NUMERICAL SOLUTION TECHNIQUE

The numerical algorithm follows the work of Erlebacher, Hussaini, and Jackson [21] and Hussaini and Erlebacher [22]. The computational domain is defined by $x \in [-120, 0]$ (excluding the buffer domain) and $r \in [0,120]$ with a grid resolution of 600×600. The domain is appropriately adjusted to accommodate vortex rings of larger and smaller aspect ratios. At the chosen resolution, there are approximately 5 points per unit length in the streamwise and the radial directions. Spatial derivatives are based on a 6th order compact difference scheme with built-in symmetry conditions at $r = 0$ to avoid loss of accuracy at the symmetry axis. Time advancement is based on a 4th-order Runge-Kutta scheme. The shock is fitted by one of the boundaries of a time-dependent curvilinear mesh. Shock fitting permits the treatment of the shock discontinuity without incurring the Gibb's phenomenon normally associated with shock capturing algorithms. The Rankine-Hugoniot conditions are used to update the flow at the shock. (Note that the shock motion does not affect the structure of the upstream flow.) The unknown shock velocity is the unknown variable in a shock evolution equation that is solved along with the equations of motion. On the downstream boundary, the flow is subsonic. The mean flow velocity is smoothly increased in a buffer domain appended to the downstream boundary to ensure a supersonic outflow boundary condition. As a result, the reflection of waves from the downstream boundary is strongly damped. Additional details of the solution technique can be found in Ding *et al*. (19).

RESULTS AND DISCUSSIONS

In this section, we discuss the influence of shock strength (M_1) and upstream disturbance amplitude (Γ) on the shock profiles, the downstream circulation, and on the downstream pressure and entropy disturbances at the shock.

Shock profiles

Figure 2 shows a series of shock displacement profiles $\delta(r)$ over time during the interaction of a $M_1 = 1.5$ shock with the vortex ring. The upstream circulation $\Gamma = 0.01$ ensures that nonlinear effects can be neglected. The profile at $t^* = 0$ is emphasized in bold. Before the vortex core reaches the shock ($t^* = -1$), the shock shape is smooth, while the shock profile has discontinuous slope at $r = r_c \pm 1$ at $t^* = 0$. This reflects the discontinuity of the vorticity at the edge of the vortex core. The shock distortion is not antisymmetric about $\delta = 0$ (which would be the case for infinite aspect ratio ring). This asymmetry results from the continuous interaction of the shock with the axisymmetric upstream irrotational velocity field built up over $t^* \in (-\infty, -1)$. For $r > r_c + 1$, the two vortex cores in the azimuthal plane have opposing effects on the shock distortion, and their mutual influence is destructive. On the other hand, in the region $r < r_c - 1$, the shock velocities induced by the two vortex cores have the same sign, thus reinforcing the shock displacement. We also note that once the center of the vortex has crossed the shock, the maximum shock displacement in the region between the two vortex cores keeps growing, while the maximum outside these vortex cores starts to decrease.

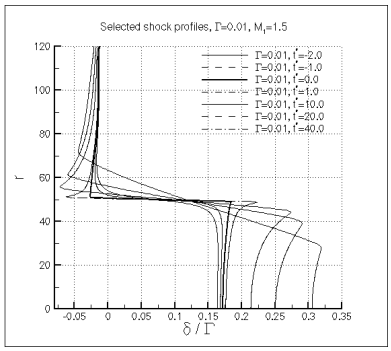

Figure 2. Selected shock profiles. M_1=1.5, Γ=10^{-2}.

In Figure 3, we plot δ / Γ for $\Gamma = 0.01$, 0.1, and 1.0 at two times ($t^* = 0$ and $t^* = 5.0$). We conclude that for $M_1 = 1.5$, the shock displacement can be modeled by linear theory.

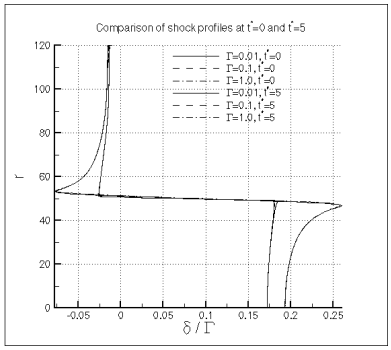

Figure 3. Effect of upstream amplitude on shock displacement. t^*=0,5, M_1=1.5, R=100, Γ=10^{-2}, 10^{-1}, 1.

Figure 4 illustrates the effect of shock strength on the displacement profile of the shock at $t^* = 0$ and $\Gamma = 0.01$. Over the range of shock Mach numbers considered, the shock displacement decreases as the Mach number is increased. This is consistent with the notion that stronger shocks are "stiffer". The variation of δ with M_1 outside $(r > r_c)$ and inside $(r < r_c)$ the vortex ring is similar, which suggests that any scaling of δ with M_1 is uniform across the shock.

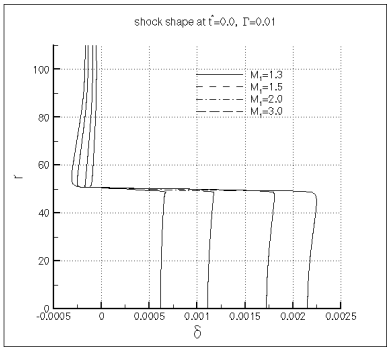

Figure 4. Comparison of shock profiles at t^*=0. R=100, Γ=0.01.

The time history of δ at two representative radii, the symmetry axis $(r=0)$ and the center of the vortex core $(r=r_c)$, are shown in Figure 5 and 6 for $M_1 \in [1.3, 3.0]$. Except for a steeper slope in the profiles of Figure 6 while the shock interacts with the vortex core, the time-variation of δ is qualitatively the same at both radii.

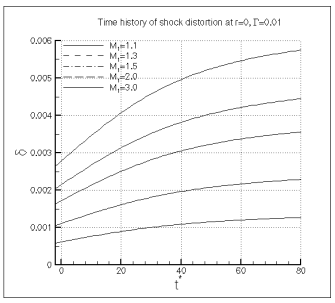

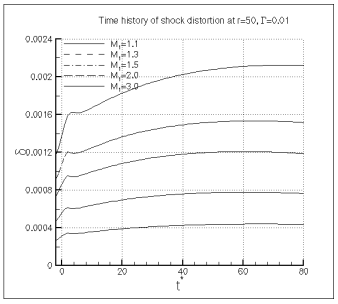

Figure 5 (left) and Figure 6 (right). Time history of shock displacement at r=0 (left) and at r=r_c (right). R=100, Γ=10^{-2}, 10^{-1}, 1.

The approximately constant curve-spacing suggests a power law scaling with the shock Mach number. The shock displacement at the symmetry axis (multiplied by $M_1^{-1.5}$) is plotted versus time in Figure 7. The profiles almost collapse to a single curve implying that the shock displacement at the symmetry axis approximately evolves as $M_1^{-1.5}$.

Downstream circulation

Figure 8 shows the time history of downstream circulation (normalized by Γ) for $M_1 = 1.5$ and several values of Γ. Clearly, the downstream circulation can be modeled as a linear process. After a sharp increase that results from the generation of the downstream vortex ring, the circulation decreases steadily. The generation of vorticity at the shock is directly related to the shock curvature and the non-uniform variation of the shock velocity. The circulation is found to decrease at a steady rate, once the upstream vortex has crossed the shock.

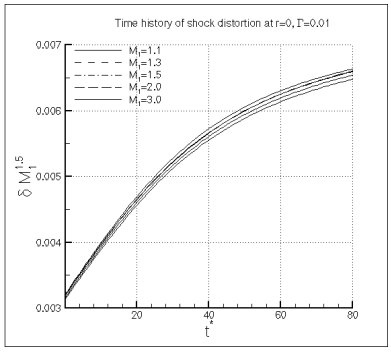

Figure 7. Time history of shock distortion at the symmetry axis, scaled with $M_1^{-1.5}$. R=100, Γ=0.01.

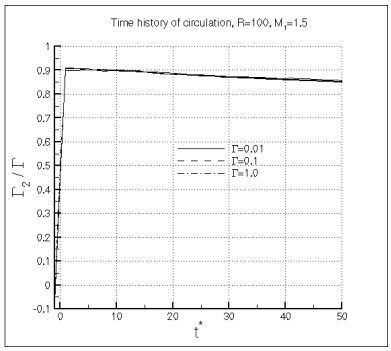

Figure 8. Time history of downstream circulation. M_1=1.5, R=100, Γ=10^{-2}, 10^{-1}, 1.

The influence of the shock strength on downstream circulation is illustrated in Figure 9. Note that the upstream circulation is not fully recovered after passage of the vortex ring through the shock. The loss of circulation increases for stronger shocks. For example, at $M_1 = 1.1$, $(\Gamma_2/\Gamma)_{\max} = 94\%$ while $(\Gamma_2/\Gamma)_{\max} = 83\%$ when $M_1 = 3$.

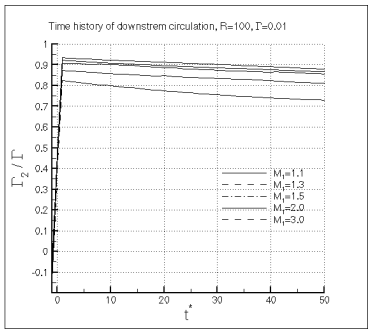

Figure 9. Time history of downstream circulation. R=100, Γ=10^{-2}.

Downstream pressure

The acoustic wave generated from a vortex ring is neither cylindrical nor spherical, but toroidal. As this wave expands away from its source (vortex ring), it eventually self-intersects on the symmetry axis, producing high amplitude pressure disturbances (19). The effect of Γ on the time history of the maximum pressure perturbation (normalized by Γ) on the symmetry axis is shown in Figure 10 for three values of Γ. Strong nonlinear effects are evident when $\Gamma = 1.0$. We do not currently know whether the nonlinearity is already present in the acoustic wave before interaction or is intensified by the interaction process itself. The maximum pressure disturbance is reached for $t^* \approx 75$.

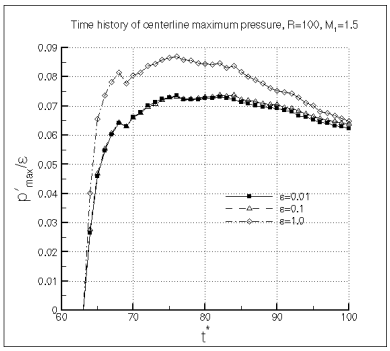

Figure 10. Time history of maximum pressure on the symmetry axis. *R*=100, Γ=10^{-2}, 10^{-1}, 1.

Figure 11 shows the time history of maximum pressure disturbance on the symmetry axis for different shock strengths. The curves are self-similar; the maximum pressure is reached at increasingly late times as M_1 is increased, and the maximum pressure amplitude scales as M_1^{α} with $\alpha > 2$, as measured between $M_1 = 1.3$ and $M_1 = 2.0$.

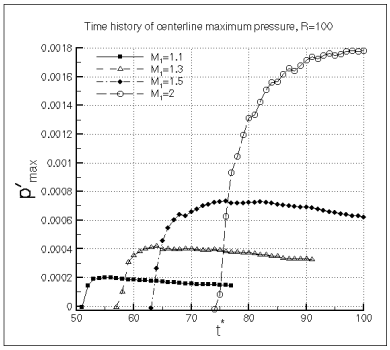

Figure 11. Time history of maximum pressure on the symmetry axis. *R*=100, Γ=10^{-2}.

Pressure, entropy and vorticity at the shock

Before the vortex core reaches the shock, the shock has interacted with the irrotational velocity field. The resulting pressure distribution at $t^* = -2$, together with several other profiles at later times, is shown in Figure 12. The precursor wave is seen on the shock as a rarefaction and a compression peak, straddled about $r = r_c$. As the vortex core crosses the shock, the pressure disturbance on the shock front increases significantly at $r = r_c \pm 1$, then propagates away from r_c at a speed $\sqrt{a^2 - u^2}$ [19], with an amplitude that scales as $1/t^*$.

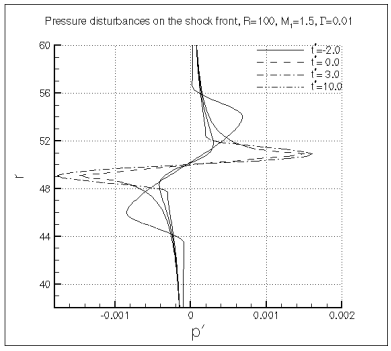

Figure 12. Pressure disturbances on the shock front. M_1=1.5, *R*=100, Γ=10^{-2}

The entropy response is qualitatively similar, but smaller in magnitude than that of the perturbation pressure. Figure 13 shows profiles of vorticity along the shock at several time instants. The production of downstream vorticity is necessarily linked to shock curvature. For $t^* < -1$, the shock is distorted by the upstream irrotational field, with a sign opposite to that of the upstream vortex. As the vortex core interacts with the shock, the vorticity at the shock is dominated by the passage of the upstream vortex core. Once the vortex core has fully crossed the shock ($t^* = 2.0$), some small amplitude vorticity (of the same sign as the main upstream vortex) is still being generated near $r = r_c$. At later time, the vorticity levels produced near r_c decrease to negligible levels, while away from r_c, there are two regions of low-level vorticity, of the same sense as that of the main vortex.

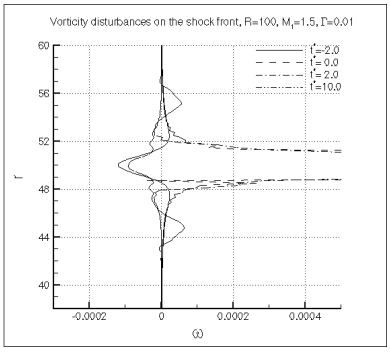

Figure 13. Vorticity on the shock front. M_1=1.5, R=100, $\Gamma=10^{-2}$.

CONCLUSIONS

The problem of a shock interaction with a vortex ring is studied numerically. Detailed investigations are carried out to investigate the influence of shock strength and upstream disturbance amplitude on the generation of downstream disturbances. We find that the shock displacement profiles behave linearly and scale as $M_1^{-1.5}$ over a large range of upstream disturbance amplitudes and a moderate range of shock strengths. The self-interaction of the acoustic wave undergoes nonlinear interactions when the upstream amplitude approaches unity. Finally, the downstream circulation behaves linearly in the range of parameters studied.

REFERENCES

1. Saffman, P. G., 1981, "Dynamics of Vorticity," Journal of Fluid Mechanics, 106, pp. 49-58.
2. Minota, T., Kambe, T. and Murakami, T., 1988, "Acoustic Emission from Interaction of a Vortex Ring with a Sphere," Fluid Dynamics Research 3, pp. 357-362.
3. Meadows, K. R., 1997, "A Study of Fundamental Shock Noise Mechanisms," NASA Technical Paper 3605.
4. Minota, T., Nishida, M. and Lee, M. G., 1997, "Shock Formation by Compressible Vortex Ring Impinging on a Wall," Fluid Dynamics Research 21, pp. 139-157.
5. Maxworty, T., 1977, "Some Experimental Studies of Vortex Rings," Journal of Fluid Mechanics, Vol. 81, pp. 465-495.
6. Glezer, A. and Coles, D., 1990, "An Experimental Study of a Turbulent Vortex Ring," Journal of Fluid Mechanics, Vol. 211, pp. 243-283.
7. Fabris, D. and Liepmann, D., 1997, "Vortex Ring Structure at Late Stages of Formation," Physics of Fluids 9(9), pp. 2801-2803.
8. Shariff, K. and Leonard, A., 1992, "Vortex Rings," Annual Review of Fluid Mechanics 24, pp. 235-279.
9. Minota, T., Nishida, M. and Lee, M. G., 1998, "Head-on Collision of Two Compressible Vortex Rings," Fluid Dynamics Research 22, pp. 43-60.
10. Minota, T., 1993, "Interactions of a Shock Wave with a High-Speed Vortex Ring," Fluid Dynamics Research 12, pp. 335-342
11. Takayama, F., Ishii, Y., Sakurai, A. and Kambe, T., 1993, "Self-Intensification in Shock Wave and Vortex interaction," Fluid Dynamics Research, 12, pp. 343-348.
12. Szumowski, A. P. and Sobieraj, G. B., 1995, "Sound Generation by a Ring Vortex-Shock Wave Interaction," AIAA Journal, Vol.34, No. 9, pp. 1948-1949.
13. Tokugawa, N., Ishii, Y., Sugano, K., Takayama, F. and Kambe, T., 1997, "Observation and Analysis of Scattering Interaction between a Shock Wave and a Vortex Ring," Fluid Dynamics Research 21, pp. 185-199.
14. Baird, J. P., 1987, "Supersonic Vortex Rings," Proceedings of the Royal Society of London A, 409, pp. 59-65.
15. Futagami,Y. and Iwamoto, J. 1996, "A Study on the Relation Between Pulsating Flow and the Noise," SAE Paper 961822.
16. Endo, M. and Iwamoto, J., 1999, "Numerical Analysis of Pulsatile Jet from Exhaust Pipe," JSAE Review 20, pp. 243-249.
17. Takayama, K., 1989, "Shock Wave Development and Propagation in Automobile Exhaust systems," SAE Transactions, 880082, pp. 4.66-4.72
18. Seiner, J. M. and Norum, T. D., 1980, "Aerodynamic Aspects of Shock Containing Jet Plumes," Sixth Aeroacoustic Conference, AIAA, pp. 1-18.
19. Ding, Z., Hussaini, M. Y., Erlebacher, G., and A. Krothapalli, 2001, "Computational Study of Shock Interaction wit a Vortex Ring, Physics of Fluids, to appear..
20. Lamb, H., 1932, Hydrodynamics, Dover New York.
21. Erlebacher, G., Hussaini, M. Y. and Jackson, T. L., 1996, "Nonlinear Strong Shock Interactions: A Shock-Fitted Approach," Theoretical Computational Fluid Mechanics, Vol. 11, No.1, pp. 1-29.
22. Hussaini, M. Y. and Erlebacher G., 1999, "Interaction of an Entropy Spot with a Shock," AIAA Journal, Vol. 37, No. 3, pp. 346-356.